Estuarine, Coastal and Shelf Science 335 (2026) 109836

Contents lists available at ScienceDirect

Estuarine, Coastal and Shelf Science

journal homepage: www.elsevier.com/locate/ecss

Spatio-temporal dynamics and socioeconomic drivers of seaport expansion in China from 1990 to 2024

Tianhao Lian [a,b], Yuanheng Sun [a,b,*], Senlin Teng [a], Xueyuan Zhu [a], Ying Li [a]

[a] Environmental Information Institute, Navigation College, Dalian Maritime University, Dalian, 116026, China
[b] State Key Laboratory of Maritime Technology and Safety, Dalian Maritime University, Dalian, 116026, China

ARTICLE INFO

Keywords:
Seaport expansion
Remote sensing
Socioeconomic drivers
XGBoost-SHAP analysis

ABSTRACT

Global trade growth has markedly increased the spatial extent of seaports in China over the past 35 years. Under the dual economic and ecological constraints, a comprehensive understanding of the processes, patterns, and drivers of seaport expansion is essential. As such, this study selected 32 major seaports in China and quantified their expansion and analyzed center of gravity migration trends with the Landsat remote sensing imagery from 1990 to 2024. Socioeconomic indicators were further integrated with Pearson's correlation analysis and an XGBoost-based SHAP approach to explore the drivers of seaport expansion. The results show that the total expansion area of the 32 seaports reached 837.17 km^2 over 35 years, with the Bohai Sea contributing the largest share. Most seaports followed an "S-shaped" growth trajectory, with rapid expansion concentrated between 2005 and 2013. Seaports along the East China Sea predominantly expanded parallel to the coastline, whereas those in other regions expanded seaward. In terms of driving forces, seaport expansion in the Bohai Sea and South China Sea regions is more strongly influenced by cargo throughput, whereas in the East China Sea region the gross domestic product (GDP) of seaport cities plays a more dominant role than cargo throughput. These findings provide a comprehensive understanding of the spatiotemporal patterns and driving mechanisms of seaport expansion in China, thereby establishing a scientific basis for future seaport development strategies and ecological management policies. At the same time, they offer critical anthropogenic context for interpreting and managing changes in estuarine and coastal systems.

1. Introduction

In the context of the rapid expansion of global trade, seaports serve as critical hubs for maritime transportation and international logistics. Their carrying capacity and level of development exert a substantial influence on national economic performance and regional competitiveness (Abdelhafez et al., 2021; Hanson and Nicholls, 2020; Verschuur et al., 2022). In China, seaports function not only as conduits for the import and export of bulk commodities but also serve as pivotal anchors for industrial clustering, spatial expansion, and infrastructure upgrades in coastal cities (J.-R. Chen et al., 2025; Yuen et al., 2013). However, seaport development necessitates acquiring the land resources required for coastal economic growth and international trade, making seaport expansion prevalent worldwide (Wang et al., 2023; Zhu et al., 2024). Among the various expansion strategies, land reclamation has historically been the predominant approach, and China accounts for the largest area of reclaimed land globally for seaport development (Martín-Antón et al., 2016). Although seaport expansion generates significant economic benefits, it also gives rise to a range of ecological and environmental challenges, including coastal ecosystem degradation, deterioration of water quality, and increased vulnerability to natural hazards (Gong et al., 2020; Sengupta et al., 2023; Wang et al., 2023; Zhu et al., 2024). Consequently, a comprehensive and scientific understanding of the processes, spatial patterns, and driving mechanisms of seaport expansion is essential for regional planning, risk assessment, ecological conservation, and the formulation of effective policy and regulatory frameworks (Sengupta and Lazarus, 2023).

The utilization of remote sensing technology has become pervasive in the domain of coastal monitoring and analysis, encompassing assessments of seaport expansion. In such contexts, the capacity to discern between water bodies and non-water bodies constitutes a pivotal step in the process. Compared with conventional methodologies, remote sensing monitoring provides several significant advantages, such as unrestricted and extensive spatial coverage, high efficiency, and low

* Corresponding author. Environmental Information Institute, Navigation College, Dalian Maritime University, Dalian, 116026, China.
E-mail address: yhsun@dlmu.edu.cn (Y. Sun).

https://doi.org/10.1016/j.ecss.2026.109836
Received 27 November 2025; Received in revised form 17 March 2026; Accepted 17 March 2026
Available online 18 March 2026

cost (Wang et al., 2019). These characteristics position it as a vital mean for long-term seaport expansion monitoring. Landsat remote sensing data encompasses a continuous time series dating back to the 1970s, making them one of the most valuable datasets for long-term environmental monitoring (Cai et al., 2020; Tian et al., 2016). Numerous researches have demonstrated that the integration of Landsat series data with a range of water body extraction methodologies can facilitate the effective monitoring of seaport expansion and shoreline changes in adjacent regions. Liu et al. (2017) employed visual interpretation, single-band thresholding, and Normalized Difference Water Index (NDWI) methods to delineate water and non-water bodies using Landsat 8 imagery in Ningbo coastal region. Ayalke et al. (2023) employed the Landsat Toolbox within ArcGIS extension software, integrating Normalized Difference Vegetation Index (NDVI) and the Cap Transformation method to extract seaport boundary changes at Dereköy Port, Turkey. Similarly, Pardo-Pascual et al. (2012) used Landsat ETM+ and TM data to extract coastal expansions for the Ports of Castelló de la Plana and Borriana in Spain, thereby demonstrating that Landsat imagery achieves water/non-water classification accuracy comparable to that obtained using high-resolution techniques.

Chinese coastal areas have undergone substantial alterations in seaport expansion over recent decades driven by rapid seaport construction and frequent land reclamation activities. Extensive studies on Chinese coastal regions or seaports have been conducted based on continuous time series remote sensing data (Chen, 1998; Chen et al., 2017; Wang et al., 2013). Lu et al. (2023) delineated seaport coastlines in the Beibu Gulf region of Guangxi Province from 1997 to 2017 with visual interpretation of Landsat imageries. Wu et al. (2024) investigated changes in coastal tidal flats in Fujian Province and identified seaport construction as a major factor influencing these areas. In order to delineate water and non-water bodies, the researchers applied the Modified Normalized Difference Water Index (MNDWI) to multi-source remote sensing data, primarily Landsat imagery. Liu et al. (2024) examined changes along the Pearl River Estuary and Hong Kong coastline from 1998 to 2021 and concluded that land reclamation, primarily driven by seaport expansion,was a major factor behind shoreline extension. They likewise used the MNDWI based on Landsat imagery to distinguish between water and non-water areas. Nevertheless, studies encompassing multiple Chinese coastal regions have generally employed coarser temporal resolutions, often using intervals of around ten years. For instance, Yan et al. (2023) examined land reclamation and shoreline changes across Chinese coastal provinces over the past four decades at a ten-year temporal resolution by using Landsat series imagery, and concluded that seaport construction has been the primary driver of land reclamation since 2000. Similarly, Wang et al. (2021) tracked shoreline changes in three major coastal development zones of China at ten-year intervals and likewise identified port-related expansion as the dominant cause of reclamation activities after 2000.It is evident that continuous time series studies are predominantly applied to localized areas, with a notable absence of seaport expansion research using continuous time series across multiple regions or the entire Chinese coastal region.

In studies of driving factors for seaport extension, Sengupta et al. (2023) analyzed the relationship between container throughput and seaport expansion area across different seaports at the global scale. Yu et al. (2025) developed a framework incorporating indicators such as port cargo throughput, urban GDP, per capita GDP, and industrial employment to assess the level of integrated development among seaports, industries, and cities. Lu et al. (2023) employed linear regression to investigate the impact of GDP on seaport expansion area. Meng et al. (2017) used partial least squares regression model, concluding that economic factors moderately influence reclamation expansion but show no direct correlation with factors like population. Li et al. (2022) applied graphical induction to explore the impact of multiple factors on various seaport types, identifying cargo demand as a critical influence across all phases of seaport development. Although seaport expansion has been increasingly constrained by environmental regulations and shoreline "red lines" in recent years, Zhu et al. (2021) determined that reclamation is predominantly influenced by seaport land use and industrial demand after examining the Bohai Sea port cluster. A collective analysis of these studies indicates that port-specific demand and economic factors constitute the primary drivers of seaport expansion. However, as seaport expansion processes are often shaped by the interplay of multidimensional factors and nonlinear mechanisms (Yan et al., 2021), traditional methods may face limitations in capturing complex relationships, making it challenging to reveal the comprehensive impact of various factors on changes in seaport area.

Based on the above review, existing studies on seaport expansion in China have primarily focused on localized coastal regions when employing continuous time-series analyses, while national-scale investigations often rely on coarse temporal intervals. Consequently, comprehensive assessments of the detailed expansion patterns and stage-specific characteristics of major Chinese seaports at the national scale remain limited. Although existing research has identified cargo demand and economic factors as key drivers of seaport expansion, these influences are frequently examined in isolation and through linear analytical approaches. While such analyses can reveal associations between these drivers and seaport expansion, they are limited in their ability to quantify the specific contributions of each factor. Furthermore, detailed investigations are typically restricted to specific regions, which constrains the possibility of systematic cross-regional comparisons. To address these limitations, this study is guided by the following research questions: (1) What are the spatiotemporal patterns and stage-specific characteristics of seaport expansion in China from 1990 to 2024? (2) How do the spatial locations and centroid migration trajectories of seaport expansion vary among different seaports? (3) Do the dominant roles of socioeconomic drivers in seaport expansion differ across distinct maritime regions?

The structure of this paper is organized as follows. Chapter 2 introduces the study area and specifies the criteria for seaport selection. Chapter 3 provides an overview of the data sources employed in the study. Methodological approaches are addressed in Chapter 4, covering the extraction of seaport expansion ranges, center of gravity migration analysis, correlation analysis, and Shapley Additive Explanations (SHAP) analysis based on Extreme Gradient Boosting (XGBoost). In Chapter 5, the findings are reported, highlighting the temporal evolution, spatial distribution, and socioeconomic drivers of sea expansion, with particular emphasis on the regional differences in driving mechanisms revealed by the SHAP results. Finally, Chapter 6 summarizes the main conclusions.

2. Study areas

The study area encompasses major seaports along Chinese coastal regions, covering four maritime zones: the Bohai Sea, the Yellow Sea, the East China Sea, and the South China Sea.

The Bohai Sea, a semi-enclosed inland sea, is characterized by high seaport density, numerous large-scale seaports and energy export terminals, as well as favorable natural geographical conditions. The region boasts over 100 existing and suitable seaport sites, including Tianjin Port and Yingkou Port, thus serving as a vital maritime gateway for northern Chinese foreign trade. The Yellow Sea is the largest marginal sea in the western Pacific and hosts two core seaports, Dalian Port and Qingdao Port. Within this region, Jiaozhou Bay constitutes a naturally superior bay area highly suitable for seaport construction. Located within this bay, Qingdao Port serves not only as a maritime transportation hub along the Yellow Sea coast but also as a key gateway for Shandong Province and parts of the Central Plains. The East China Sea contains well-developed harbors, a notable example being Shanghai Port, situated at the estuary of the Huangpu River in the lower reaches of the Yangtze River. The South China Sea ranks among the world's busiest maritime zones, carrying more than 500,000 vessels annually and

intersected by at least 37 major international shipping lanes(http://www.scspi.org/). Key seaports in this region include Shenzhen Port, Guangzhou Port, and various seaports in the Beibu Gulf of Guangxi Province. Besides, the South China Sea functions as the most critical hub and strategic chokepoint along the north-south passage of the Western Pacific Rim, constituting an extremely vital strategic transportation lifeline for China.

Seaports were selected based on statistical data of annual cargo throughput and container throughput in 2020 from the Ministry of Transport of China "National Port Cargo and Container Throughput for December 2020" (https://xxgk.mot.gov.cn/2020/jigou/zhghs/202101/t20210121_3517383.html). The inclusion of seaports was contingent upon the fulfilment of specific criteria. Firstly, container throughput had to exceed 1 million TEU (Twenty-foot Equivalent Unit). Secondly, cargo throughput had to exceed 30 million tons, with container throughput of at least 250,000 TEUs. As such, 32 seaports were selected. 8 of them are located the Bohai Sea coast, 7 along the Yellow Sea coast, 8 along the East China Sea coast, and the remaining 9 along the South China Sea coast. The spatial distribution of these seaports is shown in Fig. 1.

3. Material

3.1. Seaport vector boundary

This study delineates the approximate seaport boundaries using vector data from the OpenStreetMap platform. OpenStreetMap furnishes vector dataset for cities globally of the year 2020, with land use classified through tags such as roads, buildings, waterways, and residential areas. Areas tagged as "seaports" (or "harbor") were identified and extracted from the corresponding city-level vector data for the 32 selected seaports and then extended seaward to approximate their full spatial extent.

Fig. 1. Spatial distribution of 32 selected seaports. Red markers indicate seaports along the Bohai Sea coastline; blue denotes the Yellow Sea, orange the East China Sea, and purple the South China Sea.

3.2. Remote sensing data

In this study, Landsat remote sensing data was utilized to extract the seaport areas of 32 seaports within the study area from 1990 to 2024. The datasets utilized in this study include Landsat 9 Surface Reflectance Tier 1 (2022-2024), Landsat 8 Surface Reflectance Tier 1 (2013-2024), Landsat 7 Surface Reflectance Tier 1 (1999-2023), and Landsat 5 Surface Reflectance Tier 1 (1990-2003). These datasets from the USGS Collection 2 (C02) T1_L2 surface reflectance products which have already undergone terrain correction, geometric correction, radiometric calibration, and atmospheric correction, they are accessible through the GEE platform (Dermosinoglou and Petropoulos, 2024). The wavelength information of the Landsat bands are summarized in Table 1, with each band providing a spatial resolution of 30 m.

3.3. Statistical data

To analyze the driving factors of seaport expansion, port cargo throughput and socioeconomic indicators such as GDP, per capita GDP and the share of GDP from the tertiary sector for the cities where the seaports are located were utilized. All data were obtained from the China Economic and Social Big Data Research Platform (https://data.cnki.net/) and the China Economic Information Network (https://ceidata.cei.cn/). The data were collected on an annual basis, and the two sources were used in a complementary manner. Most statistical data cover the period from 1990 to 2024. However, data for some cities were not recorded during the early period (1990–2000). GDP data of Jinzhou, for example, are only available from 1994 onward. The measurement of cargo throughput is expressed in tons, while that of GDP is measured in billions of Chinese Yuan (CNY) and per capita GDP is reported in Chinese Yuan (CNY) per person.

4. Methodology

In this study, Landsat remote sensing imagery from 1990 to 2024 was first acquired and processed on the Google Earth Engine platform, with the data filtered using seaport vector boundaries derived from OpenStreetMap. These data were then integrated and the annual extent of each seaport was extracted using the Automated Water Extraction Index (AWEI) combined with Otsu threshold segmentation. Subsequently, the regional center of gravity for each seaport was calculated, and the spatial pattern of seaport expansion was analyzed by fitting the direction and trend of expansion with the assist of principal component analysis (PCA). Finally, Pearson's correlation analysis was employed to evaluate the relationship between seaport expansion area and various socioeconomic indicators, and XGBoost regression combined with SHAP analysis was employed to quantify the effects of these variables and reveal regional disparities in their influence. The overall methodological framework is illustrated in Fig. 2.

4.1. Seaport extent extraction

4.1.1. Calculation of the AWEI water index

This study employed AWEI, proposed by Feyisa et al. (2014) based on Landsat imagery, to differentiate water bodies from non-water areas

Table 1
Wavelength information of Landsat image bands (micrometer).

Band	Landsat5 TM	Landsat7 ETM+	Landsat8/9 OLI
Coastal			0.43-0.45
Blue	0.45-0.52	0.45-0.52	0.45-0.51
Green	0.52-0.60	0.52-0.60	0.53-0.59
Red	0.63-0.69	0.63-0.69	0.64-0.67
NIR	0.76-0.90	0.77-0.90	0.85-0.88
SWIR1	1.55-1.75	1.55-1.75	1.57-1.76
SWIR2	2.08-2.35	2.09-2.35	2.11-2.29

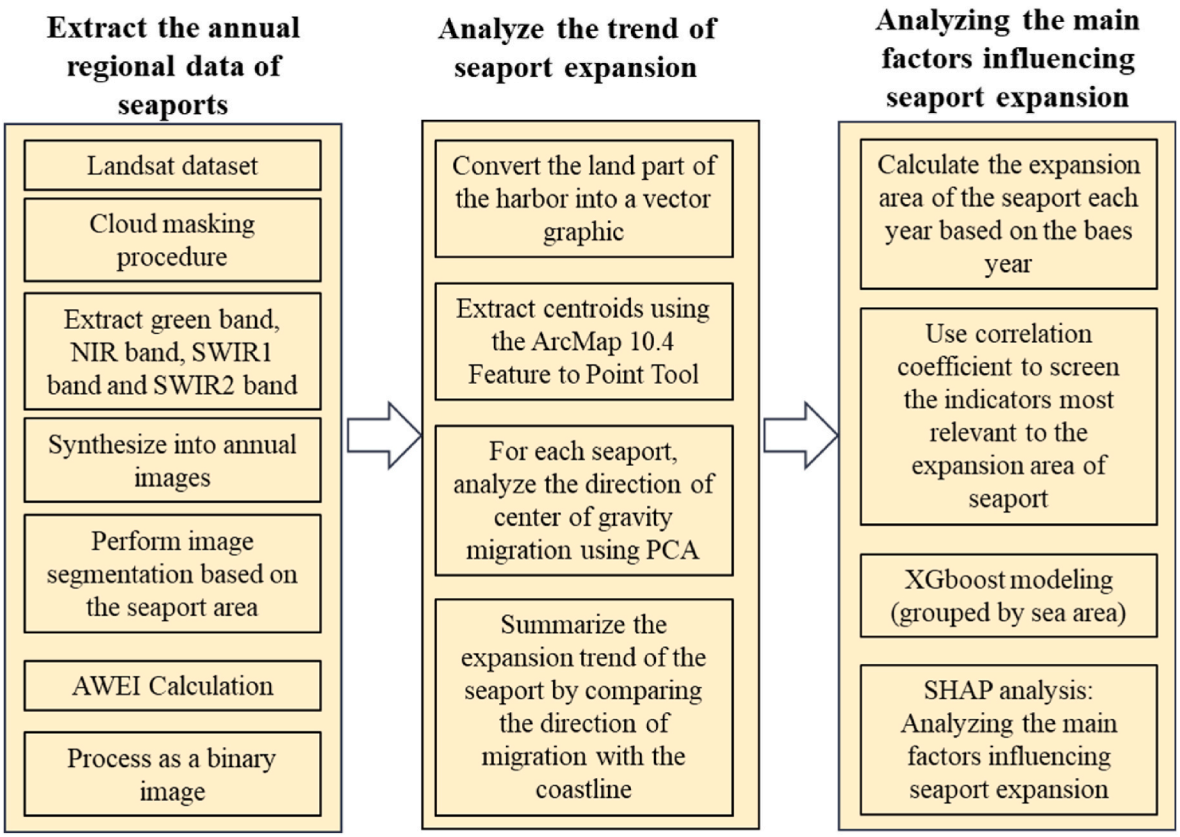

Fig. 2. Total seaport expansion area per marine region relative to 1990. The horizontal axis indicates the year, and the vertical axis depicts the cumulative expansion area of all selected seaports within each marine region since 1990.

within seaports for seaport extent extraction. Compared with traditional indices such as the NDWI and MNDWI, AWEI provides higher accuracy in delineating the edges of water bodies. Furthermore, the optimal threshold of AWEI varies less across images at different locations and times than that of MNDWI. The calculation formula of AWEI is as follows:

$$AWEI_{nsh} = 4 \times (\rho_{green} - \rho_{SWIR1}) - (0.25 \times \rho_{NIR} + 2.75 \times \rho_{SWIR2}) \quad (1)$$

Where ρ_{green} is the reflectance of the green band, ρ_{NIR} is the reflectance of the near-infrared (NIR) band, and ρ_{SWIR1} and ρ_{SWIR2} are the reflectance of the short-wave infrared (SWIR) 1 and SWIR 2 bands, respectively. All reflectance values were derived from Landsat surface reflectance data.

For a particular seaport, we imported its seaport vector boundary into GEE and retrieved all Landsat images during the non-winter season (March-October) of a year which were then screened to minimize the interference of sea ice. Then, Cloud and cloud-shadow pixels were removed, cloud masking was performed using the QA bands provided with the Landsat Collection 2 surface reflectance products (i.e. QA_PIXEL). Cloud, cloud shadow, and other invalid pixels were identified through bitwise operations, and all abnormal pixels were combined and inverted to generate a valid pixel mask(Sengupta et al., 2023). Then, we selected only the green band, NIR band, SWIR 1 and SWIR 2 bands from each image, as these bands are relevant to AWEI calculations. Subsequently, images from the same year were combined into annual composites using mean composite method, which were finally cropped according to seaport vector boundary. The AWEI was subsequently calculated from the composited image for that year.

4.1.2. Water/non-water classification based on Otsu threshold segmentation

The Otsu threshold segmentation (Sankur, 2004) is a dynamic thresholding method used to separate foreground and background. In this study, it was applied to determine the optimal threshold for distinguishing water bodies from non-water areas. This technique traverses all the pixel values of a given gray-scale image. For instance, if the currently selected pixel value is designated as t then the entirety of the pixel values present within the image are divided into two distinct classes. The pixel value that is less than or equal to t is designated as the background class, whereas those with values greater than t constitute the foreground class (Ghorai and Mahapatra, 2020).

The inter-class variance at this t value is calculated as follows:

$$\sigma_b^2 = \omega_1(t)\omega_2(t)[\mu_1(t) - \mu_2(t)]^2 \quad (2)$$

Where, $\omega_1(t)$, $\omega_2(t)$ represent the ratios of the number of pixels in each class to the total number of pixels in the image, $\mu_1(t)$, $\mu_2(t)$ is the average gray value of the two classes of pixels, and σ_b^2 is the inter-class variance.

When the inter-class variance reaches its maximum, the corresponding t-value is identified as the optimal threshold (Yang et al., 2014). After determining the optimal threshold, t_a, the image value of the region with an image value greater than t_a, i.e., the water body region, is set to 0. Conversely, the image value of the region with an image value less than t_a, i.e., the non-water body region, is set to 1. Ultimately, this process culminates in the formation of a binary image depicting the distinction between the water body and non-water body regions, thereby accomplishing the extraction of the seaport extent.

4.1.3. Accuracy assessment

To quantitatively evaluate the agreement between the AWEI-based classification results and reference data, Overall Accuracy (OA) and Cohen's Kappa coefficient were employed as an indicator of classification accuracy (Congalton, 1991). OA is the ratio of correctly classified pixels to the total number of pixels in the image. And the Kappa

coefficient is derived from the confusion matrix and accounts for both the observed agreement and the agreement expected by chance, and is defined as follows:

$$Kappa = \frac{P_0 - P_e}{1 - P_e} \tag{3}$$

In this formulation, P_0 denotes the observed agreement between the classification results and the reference data, calculated as the ratio of correctly classified pixels to the total number of pixels, whereas P_e represents the expected agreement under random classification, which is estimated from the marginal probabilities of each class. The Kappa coefficient ranges from −1 to 1.

4.2. Trend analysis of seaport center of gravity migration

In order to analyze the trend of seaport spatial expansion, this study extracted the annual center of gravity of each seaport and to fit the migration trend of the center of gravity using the PCA over the 35-year study period.

The study first converted the annual water/non-water binary images of each seaport into polygons. The geometric centers of gravity for these polygons were then calculated using the Feature to Point tools with ArcGIS Desktop 10.4 software (*ESRI*, Redlands, CA, USA). The calculation equation is expressed as follows:

$$G_x = \frac{1}{6A}\sum_{i=0}^{n-1}(x_i + x_{i+1})(x_i y_{i+1} - x_{i+1} y_i) \tag{4}$$

$$G_y = \frac{1}{6A}\sum_{i=0}^{n-1}(y_i + y_{i+1})(x_i y_{i+1} - x_{i+1} y_i) \tag{5}$$

In the formula, (x_i, y_i) represents the coordinates of the ith vertex of the polygon. A denotes the area of the polygon and (G_x, G_y) represent the coordinates of the centroid of the polygon.

The PCA was further applied to model the migration direction of each seaport's center of gravity. The fundamental principle of PCA is to identify the direction of maximum variance in the data while retaining its essential variability. Specifically, the annual coordinates of each seaport's center of gravity were arranged into a matrix X composed of two-dimensional sample points. After subtracting the mean vector, the covariance matrix C was computed, followed by eigenvalue decomposition of C to obtain the largest eigenvalue and its corresponding eigenvector v_1. The eigenvector represents the principal direction of center of gravity migration (i.e., the first principal component), while the associated eigenvalue reflects the degree of variation along this direction.

To visualize shifts in the centers of gravity, the annual coordinates of each seaport were projected onto ν_1, producing projection coefficients that were then used to construct a best-fit line representing the overall migration trend. The minimum and maximum projection coefficients defined the starting and ending points of this line. This fitted vector (i.e., visualized eigenvector ν_1) visually represents the direction of each seaport's center of gravity migration in geographic space, with its length indicating the migration distance. The calculation procedure is expressed as follows:

$$p_i = (g_i - \mu) \times \nu_1 \tag{6}$$

$$P_{start} = \mu + \min_{1 \le i \le n}(p_i) \times \nu_1 \tag{7}$$

$$P_{end} = \mu + \max_{1 \le i \le n}(p_i) \times \nu_1 \tag{8}$$

Where g_i denotes the coordinates of the ith center of gravity point (x_i, y_i), μ denotes the mean vector, p_i denotes the projection coefficients of the coordinates of g_i , P_{start} and P_{end} denote the coordinates of the start point and the end point of the fitted line.

4.3. Correlation analysis

In this study, Pearson's correlation analysis is used to explore the correlation between seaport expansion area and socio-economic indicators such as cargo throughput, GDP, per capita GDP, and the share of GDP from the tertiary sector, and the Pearson's correlation coefficient is calculated as follows:

$$r = \frac{\sum (x_i - \overline{x})(y_i - \overline{y})}{\sqrt{\sum (x_i - \overline{x})^2 (y_i - \overline{y})^2}} \tag{9}$$

Where, r is the Pearson correlation coefficient, i is the year in which the data is located, x is the socio-economic indicator, and y is the expand area. The area of seaport expansion calculated in this study is defined as the area expanded since the base year 1990.

4.4. SHAP analysis based on XGBoost

Building on the results of the correlation analysis, this study employs the SHAP analysis method based on XGBoost algorithm to evaluate the influence of certain socioeconomic indicators on seaport expansion area.

XGBoost is an extreme gradient boosting algorithm that can be implemented within a regression framework to model relationships between a target variable and its influential factors (Chen and Guestrin, 2016). In this study, four marine regions are modelled separately. Socioeconomic indicators were used as influential factors, in conjunction with the seaport expansion area as the prediction target variable. The dataset for each modeling is randomly split into training and testing sets at a ratio of 7:3, and utilizes repeated 5-fold cross-validation. After model training, predictions for the testing set are generated, and model performance is evaluated using R^2, RMSE, MAE and CV R^2. A model is deemed to be adequately robust for SHAP interpretation when the R^2 and CV R^2 values exceed 0.5, and when both the RMSE and MAE are less than half of the mean expansion areas of each seaport within its corresponding sea region.

SHAP analysis provides a consistent and interpretable framework for quantifying the contribution of each predictor to the model output (Li, 2022). It identifies the key drivers of seaport expansion, clarifies the direction of their effects on the response variable, and enables comparisons of the relative influence of different factors. By calculating Shapley values of each factor, SHAP offers an intuitive visual representation of how each socioeconomic indicator contributes to changes in seaport expansion. The calculation method is outlined as follows:

$$\delta_i = \sum_{S \subseteq \frac{N}{\{i\}}} \frac{|S|! \cdot (|N| - |S| - 1)!}{|N|!} [f(S \cup \{i\}) - f(S)] \tag{10}$$

Where δ_i is the contribution value of factor i , N is the full set of factors, S is a subset of factors that does not contain factor i and $f(S)$ is the mathematical expectation when only the factor set S is used for prediction.

5. Results and discussion

5.1. Changes of seaport area

To quantify the accuracy of the seaports area extracted using AWEI, we randomly selected multiple harbors from different years. Using high-resolution imagery from Google Earth, we conducted visual interpretation and manually delineated these seaport areas, which served as reference data for accuracy assessment. Kappa values for these areas ranged from 0.80 to 0.93, while OA values are at or above 0.95, indicating an almost perfect agreement between the extracted seaport areas

and the reference data. Although this accuracy assessment was not applied to all years for all seaports, it provides an empirical basis for evaluating the reliability of the seaport extraction approach. Given that the same Landsat data sources, preprocessing workflow, and classification criteria were consistently applied across all seaports and years, the relative comparisons and long-term expansion trends analyzed in this study are expected to be robust, even in the presence of localized classification uncertainties at finer spatial scales.

This study quantified the annual expansion area of each seaport since 1990. The results indicate that 32 major seaports along the Chinese coastline collectively expanded by 837.17 km^2 relative to their 1990 extents. Among the four coastal regions, the Bohai Sea exhibited the largest increase, with an expansion of 485.55 km^2, followed by the Yellow Sea (122.47 km^2), the East China Sea (94.33 km^2), and the South China Sea (134.81 km^2) (Fig. 3). The mean expansion areas per seaport in these regions were 60.69 km^2, 17.50 km^2, 11.79 km^2, and 14.98 km^2, respectively.

The Bohai Sea has demonstrated the highest levels of total growth and average growth per seaport. Tianjin and Tangshan Ports in the Bohai Sea were identified as the largest contributors to regional expansion, driving much of the observed change across the entire region (Fig. 4). The expansion of Tianjin Port was 170.807 km^2, and the expansion of Tangshan Port (including Jingtang Port and Caofeidian Port) was 182.474 km^2. After the exclusion of those two seaports, the average growth area per seaport of others in the Bohai Sea was 22.044 km^2, which remains the highest value among the four sea areas. Growth patterns in the Yellow Sea and East China Sea regions were relatively similar, exhibiting a less pronounced S-shaped trajectory. This pattern aligns with the development trends of major seaports in these regions, notably Qingdao Port in the Yellow Sea and Shanghai Port in the East China Sea. In the South China Sea, seaport expansion generally follows an S-shaped trajectory. Growth remained moderate from 1990 to 2004 and again from 2015 to 2024, but accelerated markedly between 2004 and 2015. This pattern is consistent with the trends observed at most seaports in the region, including Guangzhou and Qinzhou.

Most seaports experienced an accelerated growth phase between 2005 and 2013, typically following a near S-shaped trajectory characterized by slow-fast-slow expansion (see Fig. A1 in Appendix A). However, not all seaports exhibited clear S-shaped trends. For example, Rizhao and Weihai in the Yellow Sea region and Shanghai in the East China Sea region maintained relatively steady growth patterns during the past three decades.

Yantai Port in the Yellow Sea, as well as Shenzhen Port and Shantou Port in the South China Sea in the South China Sea underwent rapid expansion followed by stabilization after 2013. Newly constructed seaports after 2005, such as Panjin and Weifang in the Bohai Sea and Yancheng in the Yellow Sea, displayed accelerated growth during their initial operational phases, then stabilized after 2013.

Small-scale fluctuations in seaport expansion areas during the early period (1990–2000) for seaport such as Tianjin and Fuzhou may be attributable to several factors. First, previous studies (Wang et al., 2021, 2023; Zhu et al., 2024) indicated that seaport development and land reclamation in China progressed relatively slowly from the 1980s to the late 1990s, with limited new construction during this period. Consequently, the actual land-use areas of seaports changed only marginally. Under such conditions, automated extraction of seaport areas from satellite imagery may be susceptible to external influences, such as tidal conditions and water turbidity, which can introduce uncertainty into area estimates and produce minor fluctuations in time-series data. In addition, even during periods of overall stagnation, localized functional adjustments, such as shoreline modifications, berth extensions, or yard expansions, could still generate subtle changes in actual seaport areas. The combined effect of these factors may explain the small undulations observed in area-change curves during otherwise stable phases. After 2000, seaports entered a phase of rapid expansion. Between 2005 and 2010 in particular, reclamation activities increased sharply, with more than 70% of new land reclamation occurring along China's northern coast and about 35% concentrated in Bohai Bay. Since 2013, policies

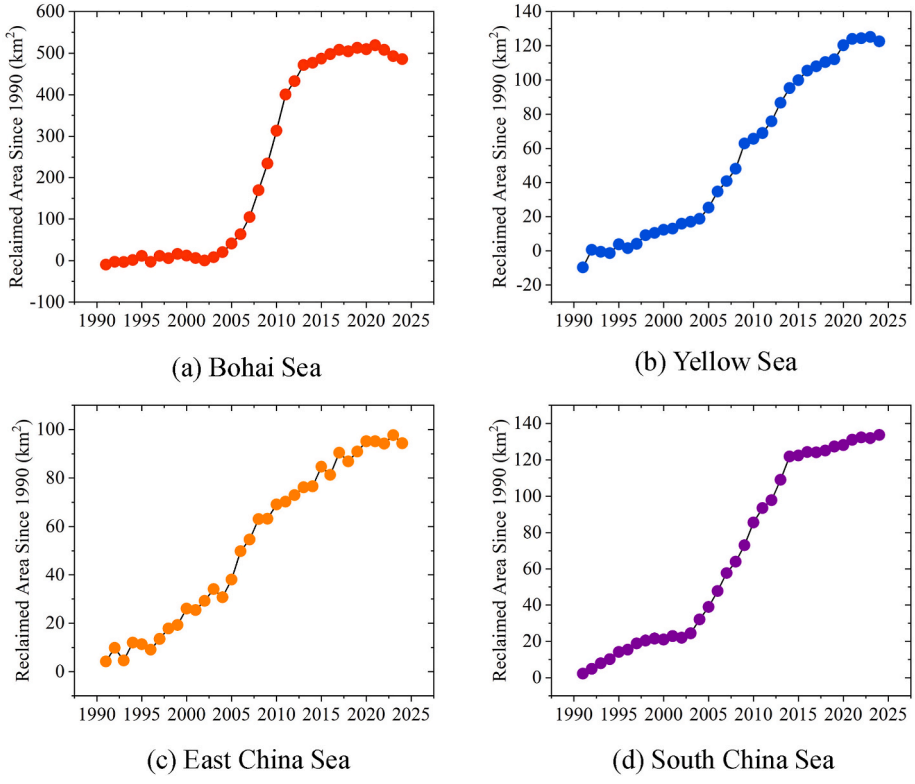

Fig. 3. Total seaport expansion area per marine region relative to 1990. The horizontal axis indicates the year, and the vertical axis depicts the cumulative expansion area of all selected seaports within each marine region since 1990.

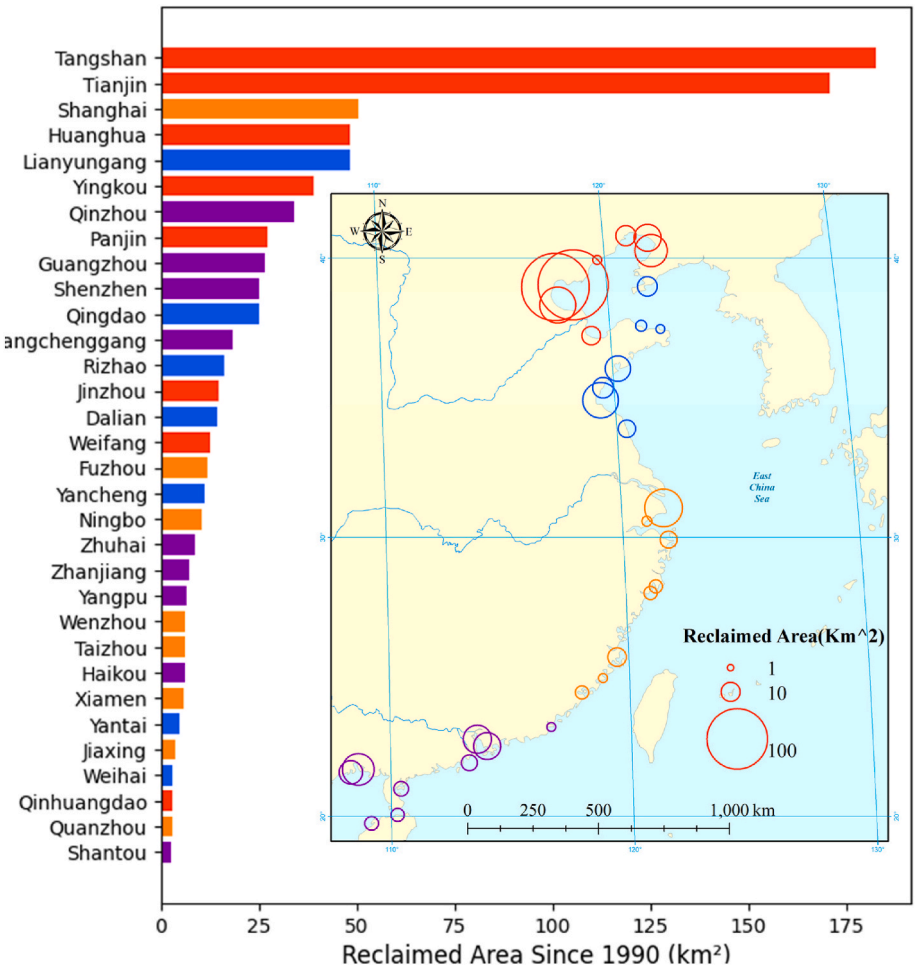

Fig. 4. Total expansion area of each seaport since 1990. Seaports in the Bohai Sea are marked in red, the Yellow Sea in blue, the East China Sea in orange, and the South China Sea in purple. In the map on the right, the size of each circle represents the magnitude of the seaport's expansion, with larger circles indicating greater expansion areas.

regulating seaport reclamation have gradually tightened, resulting in a progressive slowdown in the rate of seaport expansion. These findings are consistent with previous research (bY. Chen et al., 2025; Gong et al., 2020).

Seaports such as Tianjin and Huanghua experienced marked reductions in seaport area after 2020. Analysis of high-resolution imageries from Google Earth revealed that multiple new waterways were constructed within the Beitang Port Area, which located in Tianjin Port, during this period, and parts of the seaport area were converted from non-water to water surfaces (Fig. 5a and b). This change may reflect a shift toward internal reclamation in response to increasingly stringent restrictions on seaward seaport expansion (Wang et al., 2023). Huanghua Port also experienced a decrease in area between 2021 and 2024, primarily due to extensive silt deposition near the seaport in 2021, which caused fragmentation of the surrounding shoreline. By 2024, much of the silt had been partially removed, resulting in a more regular shoreline configuration. The cleared waters were subsequently designated as the new territorial waters of Huanghua Port, leading to an apparent landward shift of the shoreline. This adjustment was reflected in a decline in the measured seaport area. (Fig. 5c and d). For other seaports showing area decreases in certain years, detailed comparisons using multi-temporal high-resolution imageries confirm that the seaport areas extracted in this study accurately reflect the actual processes of seaport development and shoreline modification.

5.2. Spatial pattern of seaport expansion

Based on the results of seaport center of gravity migration, the expansion patterns of major seaports in China over the past 35 years are classified into four categories: simple seaward expansion, coastal expansion, uneven multi-port seaward expansion, and uniform multi-port seaward expansion.

Simple seaward expansion refers to seaports with a single seaport area that expand predominantly seaward, with the expansion vector roughly perpendicular to the coastline. Coastal expansion describes seaports originally constructed at the shoreline that continue to reclaim land along the coast rather than outward into deeper waters. Examples include Xiamen Port and Guangzhou Port at the Pearl River estuary, both of which have built multiple seaport areas progressively along the coastline. Uneven multi-port seaward expansion refers to seaports consisting of two or more relatively dispersed seaport areas, all exhibiting a general trend of simple seaward expansion. However, some seaport areas develop much more rapidly than others, resulting in a centroid migration vector that runs from one seaport area toward another and is roughly parallel to the coastline. Uniform multi-port seaward expansion describes seaports with two or more dispersed seaport areas that all expand seaward at a relatively even pace, producing a fitted vector that points directly toward the sea.

Fig. 6 delineates the seaport expansion patterns of six seaports The selected seaports which can represent four typical expansion modes. The arrows shown in the figure represent migration vectors fitted using PCA,

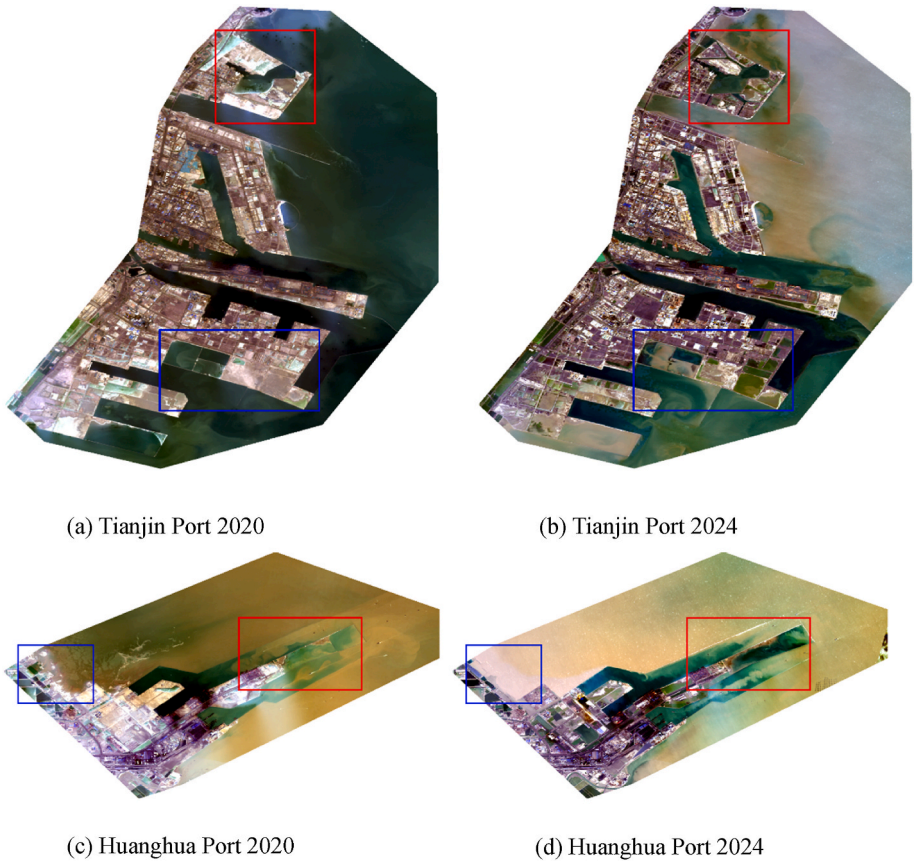

Fig. 5. Optical imagery of Tianjin Port and Huanghua Port in 2020 and 2024. Panels (a) and (b) show Tianjin Port in 2020 and 2024, respectively. The red box highlights the Beitang Port Area in Tianjin Port, while the blue box marks the main seaport area. Panels (c) and (d) depict Huanghua Port in 2020 and 2024, respectively. In these images, the red box indicates the siltation-prone zone surrounding Huanghua Port, and the blue box delineates the adjacent shoreline.

with arrow direction indicating the trajectory of expansion and arrow length denoting the migration distance.

Among the seaports examined in this study, eight are located in the Bohai Sea. Tangshan Port exhibits an uneven multi-port seaward expansion pattern, whereas the other seven, Tianjin, Qinhuangdao, Huanghua, Jinzhou, Panjin, Yingkou and Weifang, display simple seaward expansion. Seven seaports are situated in the Yellow Sea. Yantai and Rizhao show simple seaward expansion; Dalian, Qingdao, and Weihai demonstrate uniform multi-port seaward expansion; and Lianyungang and Yancheng exhibit uneven multi-port seaward expansion. In the East China Sea, eight seaports are included. Shanghai, Ningbo (main port), Jiaxing, and Xiamen are characterized by coastal expansion. Taizhou, Fuzhou, and Quanzhou display uneven multi-port seaward expansion, while only Wenzhou shows simple seaward expansion. In the South China Sea, nine seaports are considered. Zhanjiang demonstrates uneven multi-port seaward expansion; Guangzhou and Haikou are characterized by coastal expansion; Zhuhai, Fangchenggang, Qinzhou, and Yangpu follow simple seaward expansion; and Shenzhen and Shantou represent uniform multi-port seaward expansion. Overall, the selected seaports predominantly exhibit seaward expansion, whereas half of seaports in the East China Sea region, display coastal expansion patterns.

Although this study primarily focuses on seaport expansion as a land-use change process, such expansion is largely concentrated in estuarine and coastal zones and is closely associated with shoreline modification, sediment redistribution induced by dredging activities, alterations in hydrodynamic conditions, and the fragmentation of coastal habitats. Previous studies have shown that the proportion of artificial coastline along the Chinese coast has increased steadily, currently accounting for approximately two-thirds of the total coastline length (Wu et al., 2024). One of the primary drivers of this trend is seaport expansion, which directly occupies natural coastal zones such as tidal flats and coastal wetlands (Wang et al., 2023; Yan et al., 2023). Since 2000, seaport construction has become a dominant form of land reclamation, increasing shoreline sinuosity and effectively lengthening the overall coastline (Wang et al., 2021). Such direct human interventions in the coastal zone are often destructive and largely irreversible, making the restoration of original natural systems and their ecological functions extremely challenging (Liu et al., 2024). By providing spatially consistent, multi-decadal evidence of seaport expansion and its driving mechanisms, this study offers essential anthropogenic context for understanding and managing changes in estuarine and coastal systems.

5.3. Seaport expansion driver analysis

To further investigate the factors influencing seaport expansion, this study examined the relationships between seaport expansion areas and several socioeconomic indicators. The study firstly analyzed the correlation between the expansion area of each seaport with cargo throughput, GDP, per capita GDP and the share of GDP from the tertiary sector. The unit of analysis for correlation was year observations. For each seaport, annual expansion area and the corresponding socioeconomic indicators from the base year to 2024 were compiled to form a time-series dataset, and each seaport was analyzed independently. Pearson's correlation coefficient was employed to assess the strength of association between expansion area of each seaport and the socioeconomic indicators, with the results of Correlation coefficient are presented in Table 2. The specific p-values and 95% confidence interval information are presented in Appendix B. Prior to calculating the correlation coefficients, the assumptions of linearity and normality were

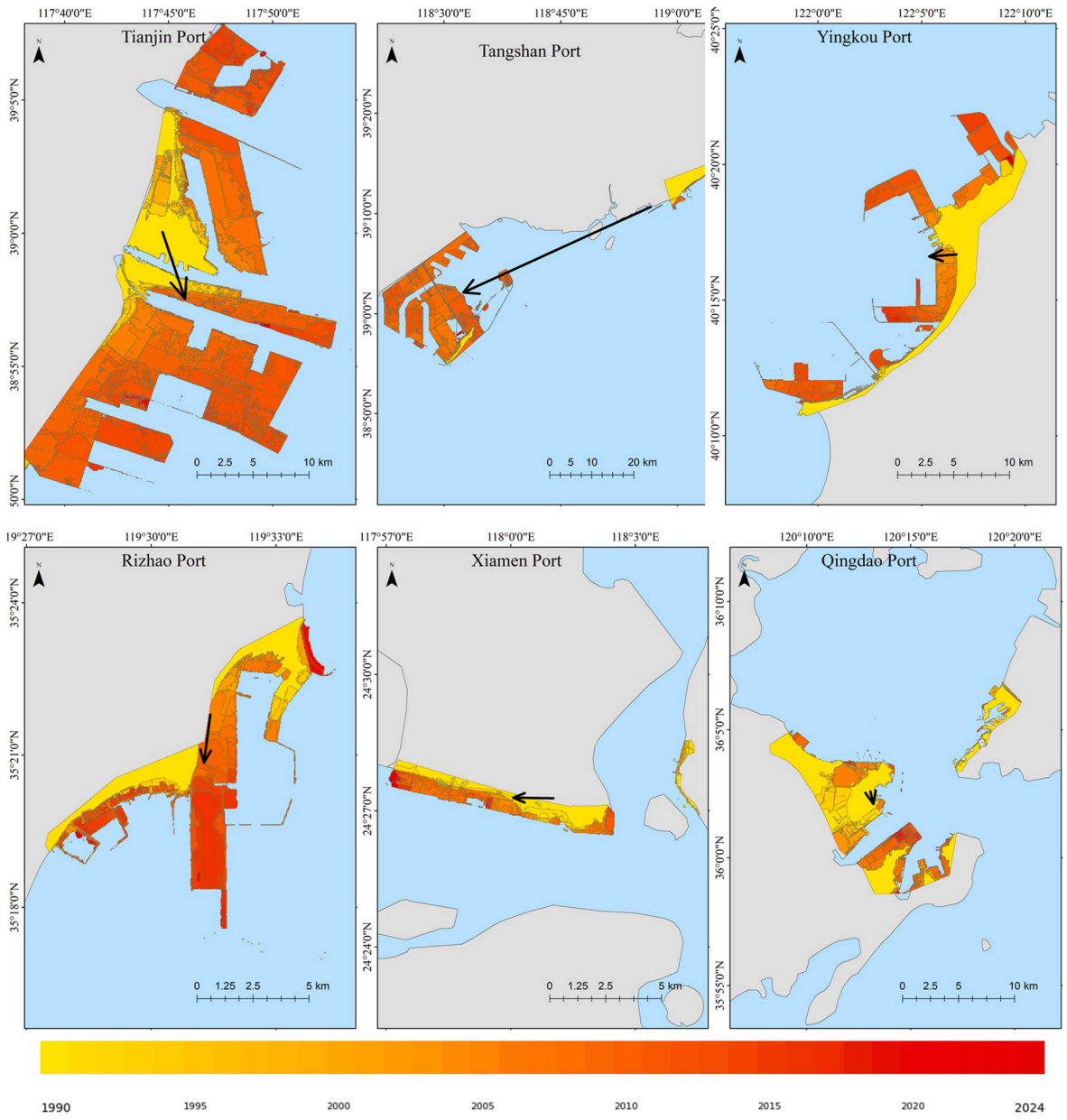

Fig. 6. Illustrative expansion patterns of six representative seaports. Colors indicate the construction period, as shown in the color bar below the figure. Tianjin Port, Yingkou Port, and Rizhao Port exhibit simple seaward expansion; Tangshan Port shows uneven multi-port seaward expansion; Xiamen Port demonstrates coastal expansion; and Qingdao Port displays uniform multi-port seaward expansion. The arrows indicate the migration direction of each seaport's center of gravity, with arrow length representing the migration distance.

examined. It was established that the seaport expansion area and the four socioeconomic indicators met the required statistical assumptions.

As illustrated in Table 2, a robust correlation exists between seaport expansion area and both cargo throughput and GDP for the most of seaports. Only a few seaports show non-significant relationships ($p > 0.05$). For example, Yancheng and Jiaxing Ports display no significant correlation between seaport expansion area and cargo throughput, likely because available cargo throughput data for these seaports cover only a limited number of years. Although Panjin Port maintains a relatively high correlation with cargo throughput, it shows low and non-significant correlations between seaport expansion area and GDP, as well as between it and per capita GDP ($R^2 < 0.3$, $p > 0.05$).

As illustrated in Figure A, Panjin Port initiated operation in 2011 and underwent a substantial seaport area expansion during the subsequent five years, subsequently reaching a state of stability after 2016. As an emerging seaport, its construction pace may be less constrained by local economic conditions while still reflecting anticipated cargo throughput demand. The correlation coefficients between seaport expansion area and the share of GDP from the tertiary sector were generally lower than the other three indicators. For instance, the coefficient for Shantou Port is below 0.1 between seaport expansion area and the share of GDP from the tertiary sector, and Fangchenggang Port even shows a negative correlation. Overall, the share of tertiary-sector GDP exhibits the weakest association with seaport expansion among the four factors considered.

From the four indicators examined, representative variables that best capture demand and economic drivers of seaport expansion were selected to further explore which factors predominantly influence seaport expansion in each marine region and to quantify the relative contributions of these two types of drivers to the expansion area. The strong correlation between seaport expansion area and cargo throughput as well as GDP provide the foundation for subsequent SHAP

Table 2
Correlation coefficient between seaport area and each socio-economic indicator.

Seaport	Cargo throughput	GDP	Per capita GDP	share of the tertiary sector
Huanghua	0.899	0.945	0.941	0.856
Jinzhou	0.916	0.95	0.96	0.741
Panjin	0.684	***0.55***	***0.28***	0.817
Qinhuangdao	0.816	0.669	0.68	0.365
Tangshan	0.888	0.919	0.956	0.77
Tianjin	0.963	0.95	0.98	0.925
Weifang	0.953	0.853	0.841	0.96
Yingkou	0.941	0.97	0.978	0.883
Dalian	0.962	0.95	0.974	0.632
Lianyungang	0.979	0.983	0.979	0.941
Qingdao	0.938	0.898	0.883	0.921
Rizhao	0.985	0.991	0.991	0.826
Weihai	0.993	0.983	0.982	0.968
Yancheng	***0.361***	0.951	0.955	0.967
Yantai	0.807	0.878	0.882	0.835
Fuzhou	0.944	0.98	0.974	0.894
Jiaxing	***0.442***	0.723	0.721	0.741
Ningbo	0.961	0.93	0.892	0.908
Quanzhou	0.975	0.942	0.93	0.691
Shanghai	0.967	0.882	0.856	0.934
Taizhou	0.807	0.946	0.859	0.818
Wenzhou	0.945	0.945	0.949	0.905
Xiamen	0.964	0.831	0.829	0.822
Fangchenggang	0.954	0.96	0.947	−0.463
Guangzhou	0.971	0.968	0.921	0.902
Haikou	0.946	0.839	0.851	0.662
Qinzhou	0.983	0.938	0.944	0.959
Shantou	0.696	0.71	0.71	***0.015***
Shenzhen	0.979	0.935	0.838	0.801
Yangpu	0.892	0.755	0.928	0.658
Zhanjiang	0.975	0.96	0.963	0.903
Zhuhai	0.969	0.96	0.906	0.872
Mean	0.889	0.895	0.884	0.792
Variance	0.022	0.011	0.018	0.039

Note: The values in italics and bold in the table indicate that their corresponding P-values are greater than 0.05.

analysis based on XGBoost. Combinations of seaport expansion area with cargo throughput or GDP that exhibited p-values below 0.05 in Table 2 were retained for the XGBoost-SHAP analysis. Before implementing SHAP, XGBoost regression models were developed separately for each of the four sea regions. Table 3 summarizes the results of the XGBoost-SHAP analysis, which quantifies the relationships between seaport expansion area and two key socioeconomic drivers, cargo throughput and GDP, across the four marine regions. Model performance metrics, including RMSE and MAE, as well as the baseline values, are reported in square kilometers. The contributions of cargo throughput and GDP derived from SHAP analysis are expressed as percentages relative to the baseline values. The unit of analysis for XGBoost-SHAP was port-year observations. For each sea area, annual expansion area and corresponding socioeconomic indicators from base year to 2024 of all seaports were used.

Taking the South China Sea as an example, the predicted baseline value for all seaports in the South China Sea is 8.54 km^2, which represents the mean expansion areas of each seaport in the South China Sea of 8.54 km^2 in the absence of any changes in any of the indicators (cargo throughput and GDP). Cargo throughput and GDP have the potential to enhance the baseline value by 70.8% and 28.1%, respectively. This finding suggests that, in the South China Sea, cargo throughput makes a larger average positive contribution to the model's predictions and thus shows the strongest association with seaport expansion, while GDP functions as a supportive factor that also positively affects seaport area expansion.

The East China Sea exhibits a distinctive pattern, as it is the only marine region where seaport expansion is predominantly influenced by GDP, with cargo throughput playing a secondary role. Overall, the modeling results for seaports in the East China Sea and South China Sea are relatively more stable, as indicated by higher R^2 values and lower RMSE and MAE. On the contrary, model performance for the Yellow Sea is relatively weak, with an R^2 value of only 0.45, suggesting that socioeconomic indicators provide limited explanatory power for seaport expansion in this region. This reduced performance may be attributed to the relatively smaller dataset available for the Yellow Sea compared to the other three marine regions. Nevertheless, the SHAP analysis remains valuable for illustrating the relative importance of the two indicators (Ponce-Bobadilla et al., 2024). These results suggest that socioeconomic indicators explain variations in seaport expansion more effectively in the southern coastal regions of China. The primary driver of seaport expansion is cargo throughput, followed by GDP. The East China Sea region is distinguished by a pronounced emphasis on economic-driven seaport expansion. In contrast, the Bohai Sea, the South China Sea, and the Yellow Sea display patterns that are more strongly associated with demand-driven expansion linked to cargo throughput. SHAP values reflect relative contribution to model prediction rather than causal effects.

The heterogeneous influence of socioeconomic drivers across coastal regions likely arises from fundamental differences in regional economic structures, development pathways, and the degree of coupling between seaports and urban economies. Previous studies of Chinese coastal cities have demonstrated that well-integrated port-city systems can substantially promote urban economic development by enhancing employment opportunities, logistics efficiency, industrial agglomeration, and trade flows, particularly in cities where seaport activities are deeply embedded within the regional economic fabric(Shan et al., 2014).

In the Yangtze River Delta, including major hubs such as Shanghai and Ningbo, seaport expansion is closely associated with advanced regional economic integration, the growth of service-oriented industries, and urban agglomeration strategies (Zhang et al., 2024). Recent evidence suggests that coordinated port-city development in this region stimulates economic growth through sustained investment in transportation infrastructure, warehousing, and logistics services, especially in economically mature seaport cities (Li et al., 2023). In contrast, seaports in the Bohai Rim and South China Sea regions tend to respond more directly to increases in cargo throughput linked to heavy industry, energy imports and exports, and global supply chains, where throughput growth constitutes a more immediate driver of terminal construction and land reclamation.

Taken together, these findings indicate that the relative importance of socioeconomic drivers revealed by the XGBoost-SHAP analysis is spatially heterogeneous rather than uniform, and is shaped by deeper structural factors, including the intensity of port-city integration, prevailing industrial compositions, and region-specific development policies. Future research could further clarify these mechanisms by incorporating additional indicators of industrial structure, policy frameworks, and levels of regional economic integration.

Table 3
Results of XGBoost-based SHAP analysis.

Region	R^2	RMSE(km^2)	MAE (km^2)	CV R^2	Baseline value(km^2)	Percentage contribution of cargo throughput	Percentage contribution of GDP
Bohai Sea	0.83	28.52	12.99	0.80	41.94	82.4	40.1
Yellow Sea	0.45	7.54	4.72	0.40	9.11	72.3	39.1
East China Sea	0.90	4.31	2.21	0.82	5.47	32.5	94.5
South China Sea	0.94	1.74	1.16	0.71	8.54	70.8	28.1

5.4. Strengths and limitations

This study presents several notable strengths in its analysis of socioeconomic drivers of seaport expansion. By integrating long-term, continuous Landsat-derived seaport expansion data with multi-source socioeconomic indicators, this study enables a consistent cross-regional comparison of driving mechanisms across 32 major seaports over a 35-year period. In particular, the application of an interpretable machine-learning framework combining XGBoost and SHAP allows for the quantification of the relative contributions and directional effects of key drivers under potentially nonlinear relationships, which is difficult to achieve using traditional linear regression approaches. However, this study has several limitations.

First, uncertainties are associated with long-term remote sensing–based change detection. The 30 m spatial resolution of Landsat imagery and uncertainties in water-index thresholding may introduce local-scale boundary deviations, particularly in regions affected by tidal fluctuations, high turbidity, or intensive shoreline engineering. These factors may lead to partial mismatches between extracted seaport boundaries and actual land-use extents at fine spatial scales. Second, limitations are associated with the socioeconomic driver analysis. The socioeconomic indicators are largely derived from city-level statistics, making it difficult to disentangle the independent contributions of seaports from surrounding industrial clusters. In addition, some seaports lack early-year data, which may influence the stability of long-term statistical relationships. Third, Due to data availability, policy and environmental regulatory variables were not explicitly included. the driving-mechanism assessment incorporates only macro-level variables such as cargo throughput and GDP, without explicitly accounting for factors such as policy regulations, ecological constraints, or shifts in international shipping patterns, thereby limiting the model's ability to explain complex nonlinear processes. Future studies may incorporate policy indices or environmental constraint indicators. In addition, accuracy assessment was conducted for a limited number of representative seaports in a single recent year due to data availability constraints. While this may not fully capture temporal variations in classification uncertainty, it provides a conservative estimate of extraction reliability. Finally, although the spatial and temporal framework covers all major Chinese seaports, this study does not examine intra-port functional zoning, ecological impacts, or future development scenarios in depth; these aspects warrant further investigation in subsequent research.

Despite these limitations, the consistency of the remote sensing framework, the multi-decadal observation period, and the multi-regional comparative design provide robust evidence for large scale spatio-temporal expansion patterns of Chinese seaports.

6. Conclusion

In this study, spatio-temporal expansion pattern and driving mechanism of 32 major coastal seaports in China were investigated using time-series Landsat remote sensing imagery and multi-source socioeconomic data spanning from 1990 to 2024. The results show that the total area of Chinese major coastal seaports has expanded by 37.166 km^2, with the Bohai Sea region accounting for more than half of this expansion. Most seaports exhibits an “S-shaped” growth trajectory, characterized by an initial slow expansion phase, followed by rapid growth, and subsequent stabilization. The peak expansion period occurred between 2005 and 2013, largely driven by rapid economic development and relatively relaxed policy constraints. After 2013, expansion rates generally decelerated due to the implementation of policy restrictions. Center of gravity migration analysis reveals that seaports exhibit distinct expansion patterns, including simple seaward expansion, coastal expansion, uneven multi-port seaward expansion, and uniform multi-port seaward expansion. Seaports in the East China Sea predominantly expanded along the coastline, whereas seaports in other regions extended longitudinally and further seaward. Correlation and XGBoost-SHAP analyses identified cargo throughput and GDP as the primary drivers of seaport expansion. In the South China Sea and the Bohai Sea, cargo throughput appears to be the most strongly associated factor with seaport expansion. which is “demand-led”. In contrast, seaports in the East China Sea are more influenced by GDP, which is characterized by “economic development-led”.

CRediT authorship contribution statement

Tianhao Lian: Conceptualization, Data curation, Formal analysis, Investigation, Methodology, Writing – original draft. **Yuanheng Sun:** Conceptualization, Funding acquisition, Supervision, Writing – review & editing. **Senlin Teng:** Investigation, Methodology. **Xueyuan Zhu:** Investigation, Supervision. **Ying Li:** Software, Visualization.

Declaration of competing interest

The authors declare that they have no known competing financial interests or personal relationships that could have appeared to influence the work reported in this paper.

Acknowledgements

This work is supported by the National Natural Science Foundation of China (42301391), Liaoning Young Elite Scientists Sponsorship Program of China, and Fundamental Research Funds for the Central Universities in China (3132025120).

Appendix A. Supplementary data

Supplementary data to this article can be found online at https://doi.org/10.1016/j.ecss.2026.109836.

Data availability

Data will be made available on request.

References

Abdelhafez, M.A., Ellingwood, B., Mahmoud, H., 2021. Vulnerability of seaports to hurricanes and sea level rise in a changing climate: a case study for mobile. AL. Coastal Engineering 167, 103884. https://doi.org/10.1016/j.coastaleng.2021.103884.

Ayalke, Z.G., Şişman, A., Akpinar, K., 2023. Shoreline extraction and analyzing the effect of coastal structures on shoreline changing with remote sensing and geographic information system: case of Samsun, Turkey. Reg. Stud. Mar. Sci. 61, 102883. https://doi.org/10.1016/j.rsma.2023.102883.

Cai, L., Zhou, M., Liu, J., Tang, D., Zuo, J., 2020. HY-1C observations of the impacts of Islands on suspended sediment distribution in zhoushan coastal waters, China. Remote Sens. 12, 1766. https://doi.org/10.3390/rs12111766.

Chen, L.C., 1998. Detection of shoreline changes for tideland areas using multi-temporal satellite images. Int. J. Rem. Sens. 19, 3383–3397. https://doi.org/10.1080/014311698214055.

Chen, J.-R., Choi, J.-W., Seo, Y.-J., 2025. Environmental efficiency assessment of coastal ports in China: implications for sustainable port management. Mar. Pollut. Bull. 211, 117436. https://doi.org/10.1016/j.marpolbul.2024.117436.

Chen, W., Wang, D., Huang, Y., Chen, L., Zhang, L., Wei, X., Sang, M., Wang, F., Liu, J., Hu, B., 2017. Monitoring and analysis of coastal reclamation from 1995–2015 in Tianjin Binhai New Area, China. Sci. Rep. 7, 3850. https://doi.org/10.1038/s41598-017-04155-0.

Chen, Y., Li, Y., Shou, Y., Liu, Boqun, Li, H., Liu, Bin, Chen, S., Dong, S., 2025. Exploring the ecological impacts and implementation strategies of reclamation in Taiping Bay of Dalian port as an example. J. Taiwan Inst. Chem. Eng. 166, 105023. https://doi.org/10.1016/j.jtice.2023.105023.

Chen, T., Guestrin, C., 2016. XGBoost: a scalable tree boosting system. In: Proceedings of the 22nd ACM SIGKDD International Conference on Knowledge Discovery and Data Mining. Presented at the KDD '16: the 22nd ACM SIGKDD International Conference on Knowledge Discovery and Data Mining, ACM, San Francisco California USA, pp. 785–794. https://doi.org/10.1145/2939672.2939785.

Congalton, R.G., 1991. A review of assessing the accuracy of classifications of remotely sensed data. Rem. Sens. Environ. 37, 35–46. https://doi.org/10.1016/0034-4257(91)90048-B.

Dermosinoglou, A., Petropoulos, G.P., 2024. Exploring long term impervious surface areas (ISA) dynamics using landsat imagery, Machine Learning and GEE: the case of

Attica, Greece. Remote Sens. Appl.: Society and Environment 36, 101338. https://doi.org/10.1016/j.rsase.2024.101338.
Feyisa, G.L., Meilby, H., Fensholt, R., Proud, S.R., 2014. Automated water extraction index: a new technique for surface water mapping using landsat imagery. Rem. Sens. Environ. 140, 23–35. https://doi.org/10.1016/j.rse.2013.08.029.
Ghorai, D., Mahapatra, M., 2020. Extracting shoreline from satellite imagery for GIS analysis. Remote Sens Earth Syst Sci 3, 13–22. https://doi.org/10.1007/s41976-019-00030-w.
Gong, L., Xiao, Y., Jiang, C., Zheng, S., Fu, X., 2020. Seaport investments in capacity and natural disaster prevention. Transport. Res. Transport Environ. 85, 102367. https://doi.org/10.1016/j.trd.2020.102367.
Hanson, S.E., Nicholls, R.J., 2020. Demand for ports to 2050: climate policy, growing trade and the impacts of sea-level rise. Earths Future 8. https://doi.org/10.1029/2020EF001543 e2020EF001543.
Li, Z., 2022. Extracting spatial effects from machine learning model using local interpretation method: an example of SHAP and XGBoost. Comput. Environ. Urban Syst. 96, 101845. https://doi.org/10.1016/j.compenvurbsys.2022.101845.
Li, Z., Luan, W., Wang, X., Wan, S., Su, M., Zhang, Z., 2022. Spatial expansion regular pattern and driving factors of estuarine and coastal harbors. Ocean Coast Manag. 216, 105980. https://doi.org/10.1016/j.ocecoaman.2021.105980.
Li, Z., Luan, W., Zhang, Z., Su, M., 2023. Research on the interactive relationship of spatial expansion between estuarine and coastal port cities. Land 12, 371. https://doi.org/10.3390/land12020371.
Liu, Y., Feng, J., Cheng, Q., Tsou, J.Y., Huang, B., Ji, C., Yang, Y., Zhang, Y., 2024. Investigating spatiotemporal coastline changes and impacts on coastal zone management: a case study in pearl river Estuary and Hong Kong's coast. Ocean Coast Manag. 257, 107354. https://doi.org/10.1016/j.ocecoaman.2024.107354.
Liu, Y., Wang, X., Ling, F., Xu, S., Wang, C., 2017. Analysis of coastline extraction from Landsat-8 OLI imagery. Water 9, 816. https://doi.org/10.3390/w9110816.
Lu, J., Zhang, Y., Shi, H., Lv, X., 2023. Spatio-temporal changes and driving forces of reclamation based on remote sensing: a case study of the Guangxi Beibu Gulf. Front. Mar. Sci. 10, 1112487. https://doi.org/10.3389/fmars.2023.1112487.
Martín-Antón, M., Negro, V., Del Campo, J.M., López-Gutiérrez, J.S., Esteban, M.D., 2016. Review of coastal land reclamation situation in the world. J. Coast Res. 75 (1), 667–671. https://doi.org/10.2112/SI75-133.
Meng, W., Hu, B., He, M., Liu, B., Mo, X., Li, H., Wang, Z., Zhang, Y., 2017. Temporal-spatial variations and driving factors analysis of coastal reclamation in China. Estuar. Coast Shelf Sci. 191, 39–49. https://doi.org/10.1016/j.ecss.2017.04.008.
Pardo-Pascual, J.E., Almonacid-Caballer, J., Ruiz, L.A., Palomar-Vázquez, J., 2012. Automatic extraction of shorelines from landsat TM and ETM+ multi-temporal images with subpixel precision. Rem. Sens. Environ. 123, 1–11. https://doi.org/10.1016/j.rse.2012.02.024.
Ponce-Bobadilla, A.V., Schmitt, V., Maier, C.S., Mensing, S., Stodtmann, S., 2024. Practical guide to SHAP analysis: explaining supervised machine learning model predictions in drug development. Clin. Transl. Sci. 17, e70056. https://doi.org/10.1111/cts.70056.
Sankur, B., 2004. Survey over image thresholding techniques and quantitative performance evaluation. J. Electron. Imag. 13, 146. https://doi.org/10.1117/1.1631315.
Sengupta, D., Choi, Y.R., Tian, B., Brown, S., Meadows, M., Hackney, C.R., Banerjee, A., Li, Y., Chen, R., Zhou, Y., 2023. Mapping 21st century global coastal land reclamation. Earths Future 11. https://doi.org/10.1029/2022EF002927 e2022EF002927.
Sengupta, D., Lazarus, E.D., 2023. Rapid seaward expansion of seaport footprints worldwide. Commun. Earth Environ. 4, 440. https://doi.org/10.1038/s43247-023-01110-y.
Shan, J., Yu, M., Lee, C.-Y., 2014. An empirical investigation of the seaport's economic impact: evidence from major ports in China. Transport. Res. E Logist. Transport. Rev. 69, 41–53. https://doi.org/10.1016/j.tre.2014.05.010.
Tian, B., Wu, W., Yang, Z., Zhou, Y., 2016. Drivers, trends, and potential impacts of long-term coastal reclamation in China from 1985 to 2010. Estuar. Coast Shelf Sci. 170, 83–90. https://doi.org/10.1016/j.ecss.2016.01.006.
Verschuur, J., Koks, E.E., Hall, J.W., 2022. Ports' criticality in international trade and global supply-chains. Nat. Commun. 13, 4351. https://doi.org/10.1038/s41467-022-32070-0.
Wang, N., Zhu, G., Li, X., Cheng, J., Yi, W., Liu, S., Xie, Z., 2023. Transitions and suggestions for China's coastal port reclamation policies. Ocean Coast Manag. 236, 106532. https://doi.org/10.1016/j.ocecoaman.2023.106532.
Wang, X., Yan, F., Su, F., 2021. Changes in coastline and coastal reclamation in the three most developed areas of China, 1980–2018. Ocean Coast Manag. 204, 105542. https://doi.org/10.1016/j.ocecoaman.2021.105542.
Wang, X.-Z., Zhang, H.-G., Fu, B., Shi, A., 2013. Analysis on the coastline change and erosion-accretion evolution of the Pearl River Estuary, China, based on remote-sensing images and nautical charts. J. Appl. Remote Sens. 7, 073519. https://doi.org/10.1117/1.JRS.7.073519.
Wang, X.G., Su, F.Z., Zhang, J.J., Cheng, F., Hu, W.Q., Ding, Z., 2019. Construction land sprawl and reclamation in the Johor river Estuary of Malaysia since 1973. Ocean Coast Manag. 171, 87–95. https://doi.org/10.1016/j.ocecoaman.2019.01.006.
Wu, W., Zhang, M., Chen, C., Chen, Z., Yang, H., Su, H., 2024. Coastal reclamation shaped narrower and steeper tidal flats in Fujian, China: evidence from time-series satellite data. Ocean Coast Manag. 247, 106933. https://doi.org/10.1016/j.ocecoaman.2023.106933.
Yan, F., Wang, X., Huang, C., Zhang, J., Su, F., Zhao, Y., Lyne, V., 2023. Sea reclamation in mainland China: process, pattern, and management. Land Use Policy 127, 106555. https://doi.org/10.1016/j.landusepol.2023.106555.
Yan, J., Xiao, R., Su, F., Bai, J., Jia, F., 2021. Impact of port construction on the spatial pattern of land use in coastal zones based on CLDI and LUT models: a case study of qingdao and Yantai. Remote Sens. 13, 3110. https://doi.org/10.3390/rs13163110.
Yang, K., Li, M., Liu, Y., Cheng, L., Duan, Y., Zhou, M., 2014. River delineation from remotely sensed imagery using a multi-scale classification approach. IEEE J. Sel. Top. Appl. Earth Obs. Rem. Sens. 7, 4726–4737. https://doi.org/10.1109/JSTARS.2014.2309707.
Yu, T., Li, H., Zhou, T., Zhao, N., Yang, Z., 2025. Evaluation and strategy development of port-industry-city integration: a China's case. Research in Transportation Business & Management 60, 101375. https://doi.org/10.1016/j.rtbm.2025.101375.
Yuen, A.C., Zhang, A., Cheung, W., 2013. Foreign participation and competition: a way to improve the container port efficiency in China? Transport. Res. Pol. Pract. 49, 220–231. https://doi.org/10.1016/j.tra.2013.01.026.
Zhang, J.-Q., Woo, S.-H., Li, K.X., 2024. Port-city synergism and regional development policy: evidence from the yangtze river region. Transport. Res. E Logist. Transport. Rev. 192, 103817. https://doi.org/10.1016/j.tre.2024.103817.
Zhu, G., Xie, Z., Xu, H., Liang, M., Cheng, J., Gao, Y., Zhang, L., 2021. Land reclamation pattern and environmental regulation guidelines for port clusters in the Bohai Sea, China. PLoS One 16, e0259516. https://doi.org/10.1371/journal.pone.0259516.
Zhu, G., Zhao, P., Zhang, L., Li, X., Ding, W., Yu, H., Zhang, N., Yang, S., Zhang, C., Xie, Z., 2024. Territorial spatial suitability assessment and optimization of coastal port reclamation in China. Ocean Coast Manag. 254, 107189. https://doi.org/10.1016/j.ocecoaman.2024.107189.